Tribenzotriquinacene Receptors for C_{60} Fullerene Rotors: Towards C_3 Symmetrical Chiral Stators for Unidirectionally Operating Nanoratchets

Björn Bredenkötter,[a] Maciej Grzywa,[a] Mohammad Alaghemandi,[b] Rochus Schmid,[b] Wouter Herrebout,[c] Patrick Bultinck,[d] and Dirk Volkmer*[a]

Abstract: The synthesis of a stereochemically pure concave tribenzotriquinacene receptor (**7**) for C_{60} fullerene, possessing C_3 point group symmetry, by threefold condensation of C_2-symmetric 1,2-diketone synthons (**5**) and a hexaaminotribenzotriquinacene core (**6**) is described. The chiral diketone was synthesized in a five-step reaction sequence starting from C_{2h}-symmetric 2,6-di-tert-butylanthracene. The highly diastereo-discriminating Diels–Alder reaction of 2,6-di-tert-butylanthracene with fumaric acid di(−)menthyl ester, catalyzed by aluminium chloride, is the relevant stereochemistry introducing step. The structure of the fullerene receptor was verified by ^{1}H and ^{13}C NMR spectroscopy, mass spectrometry and single crystal X-ray diffraction. VCD and ECD spectra were recorded, which were corroborated by ab initio DFT calculations, establishing the chiral nature of **7** with about 99.7% ee, based on the ee (99.9%) of the chiral synthon (**1**). The absolute configuration of **7** could thus be established as all-S [(2S,7S,16S,21S,30S,35S)-(**7**)]. Spectroscopic titration experiments reveal that the host forms 1:1 complexes with either pure fullerene (C_{60}) or fullerene derivatives, such as rotor 1′-(4-nitrophenyl)-3′-(4-N,N-dimethylaminophenyl)-pyrazolino[4′,5′:1,2][60]fullerene (**R**). The complex stability constants of the complexes dissolved in $CHCl_3/CS_2$ (1:1 vol.%) are $K([C_{60}\subset 7]) = 319(\pm156)$ M^{-1} and $K([R\subset 7]) = 110(\pm50)$ M^{-1}. With molecular dynamics simulations using a first-principles parameterized force field the asymmetry of the rotational potential for [$R\subset 7$] was shown, demonstrating the potential suitability of receptor **7** to act as a stator in a unidirectionally operating nanoratchet.

Introduction

In the last decades the construction of nanosized motors and machines has gained considerable interest.[1] An emerging part of this research is the production and operation of unidirectional molecular rotors and ratchets. From the point of view of a chemist acting as (nano-)mechanical engineer, there are two prevailing aspects in this scenario, namely: 1) the design of suitable (preferentially self-assembling) construction parts of the molecular machinery as well as, 2) the operation of the latter under appropriate (i.e., nonequilibrium) conditions.[2] In order to achieve unidirectional rotation several strategies have been suggested in the literature. An electron triggered motion, for instance, was demonstrated with appropriate scorpionate stators and ruthenium cyclopentadienyl rotors.[3] Unidirectional rotation around a single bond driven by chemical energy was realized in sterically hindered triptycene and naphthyl derivatives.[4] In these systems up to four different chemical reactions are necessary for a 360° rotation. Another family of unidirectional rotors is driven by photochemical reaction steps.[5] The rotation in these systems is initiated by photoinduced cis–trans isomerization, which results in a 180° rotation of the C=C double bond. A subsequent thermally controlled inversion of the helix structure of the molecule inhibits the back-rotation. With an additional chemical step, a clockwise and anticlockwise rotation of an appropriate rotor and an electrically driven directional motion of a "car-like" fluorene-based four-wheeled molecule was shown to be feasible.[6,7] Fluorene-based light-driven rotary motors have also been investigated in molecular modeling studies.[8] Since the former operation conditions lead to machines working rather slowly (requiring from several seconds up to many hours to complete a single rotation) alternative scenarios have been proposed recently, which suggest rotary nanoratchet systems enabled mainly by electric energy,

[a] Dr. B. Bredenkötter, Dr. M. Grzywa, Prof. Dr. D. Volkmer
Augsburg University, Institute of Physics
Chair of Solid State and Materials Chemistry
Universitätsstrasse 1, 86159 Augsburg (Germany)
E-mail: dirk.volkmer@physik.uni-augsburg.de

[b] Dr. M. Alaghemandi, Dr. R. Schmid
Ruhr University Bochum, Chair of Inorganic Chemistry 2
Computational Materials Chemistry Group
Universitätsstrasse 150, 44801 Bochum (Germany)

[c] Prof. Dr. W. Herrebout
Department of Chemistry, University of Antwerp
Groenenborgerlaan 171, 2020 Antwerp (Belgium)

[d] Prof. Dr. P. Bultinck
Department of Inorganic and Physical Chemistry, Ghent University
Krijgslaan 281-S3, 9000 Gent (Belgium)

for example, a linear polarized ac field,[9] which should yield much higher rotational frequencies. Relating to the latter approach we have designed a novel self-assembling supramolecular host–guest system, which is based on a C_3-symmetrical (chiral) tribenzotriquinacene host (7) acting as stator, which—if combined with a suitable C_{60} rotor—could act as unidirectional nanoratchet (Scheme 1).
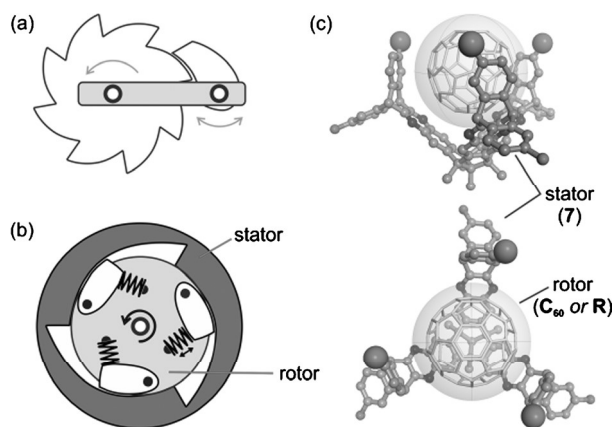
Scheme 1. a) Simple mechanical ratchet featuring a gear and a pawl mounted on a base. b) Alternative ratchet design in which the gearwheel is set in a molding shaped to admit rotation in one direction only. c) Nanoratchet design comprising the C_3-symmetrical (chiral) tribenzotriquinacene stator (7, spheres point to the position of bulky substituents, for example, *tert*-butyl groups), and a (putative) C_{60} fullerene-based rotor R[10] (Figure 7). Hydrogen atoms are omitted for clarity.

C_{60} fullerene-based devices are among the most intensively investigated systems, owing to the fact that their spherical shape should admit their usage as fundamental building blocks in future molecular mechanical devices.[11] Our previous report[12] on the test case of a simple nanosized ball joint provided a first glimpse at the rather fundamental question as to how mechanically linked components of molecular machines might be scaled down to nanosized dimensions, where quantum effects play the dominant role and the separate parts have to self-assemble spontaneously into the complete and functional device. We pointed out that C_{60} (and its derivatives) might serve the obvious purpose of the spherical ball head, but the appropriate molecular design of a shape complementary ball socket was found to be a nontrivial task. Among diverse practical issues, experimental work often shows that limited solubility of the building components imposes severe limitations on the assembly process of nanosized devices. For a suitable system the fullerene receptor should form a 1:1 complex of the composition [C_{60}⊂receptor] displaying a sufficiently large complex stability constant under the chosen experimental conditions.[12–14] Extending these studies, we here focus our investigations on the design and directed (i.e., stereoselective) synthesis of C_3-symmetrical (chiral) tribenzotriquinacene stators, which are crucial yet unexplored components of a nanoratchet system featuring unidirectional rotation. We also present the first results on the self-assembly of chiral stator (7) with fullerene-type rotors, in conjunction with molec-

ular dynamics (MD) simulations, demonstrating the asymmetry of the rotational energy profile for a rotor like R.[10]

Results and Discussion

Synthesis of the chiral receptor (7)

We herein report the synthesis of the first chiral and enantiopure tribenzotriquinacene receptor 7 for C_{60} fullerene possessing C_3 point group symmetry (Scheme 1). The C_3 symmetry of 7 is induced by *tert*-butyl substituents placed at appropriate positions of the tribenzotriquinacene moiety. Our approach towards enantiopure tribenzotriquinacene derivatives, is based on the threefold condensation of a bisaryl anellated bicyclo-[2.2.2]octane-2,3-dione with hexaaminotetramethyl tribenzotriquinacene (6; Scheme 2).
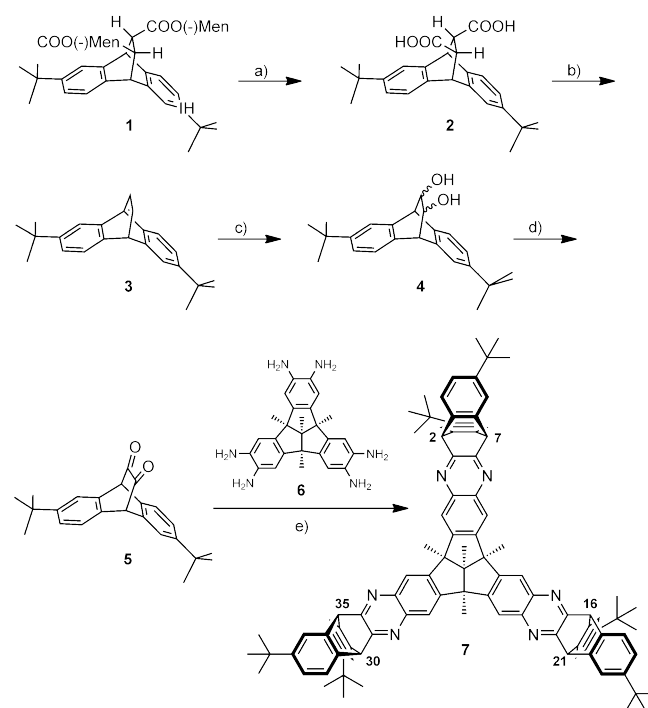
Scheme 2. Synthetic route towards receptor 7: a) 1. NaOH, EtOH, reflux, 72 h; 2. HCl, 85%; b) Pb(OAc)$_4$/Cu(OAc)$_2$, pyridine$_{abs}$/toluene$_{abs}$, reflux, 45 min, 29%; c) OsO$_4$ (cat.), NMO, acetone, RT, 15 h, 62%; d) Swern oxidation (1. TFAA, DMSO$_{abs}$/CH$_2$Cl$_{2abs}$, −78 °C, 90 min, TMA→RT, 2. HCl), 98%; e) 6 equiv 5, TFA (cat.), CHCl$_3$, water trapping, 69%.

The use of the appropriate chiral C_2-symmetric 1,2-diketone 5 for this trimerizing condensation results in the exclusive formation of one stereoisomer of receptor 7. Kräutler et al.[15] previously reported the AlCl$_3$-catalyzed [4+2] cycloaddition of 2,6-di-*tert*-butylanthracene with di-(−)-menthylfumarate to stereochemically pure di[(1R)-menthyl] (9S,10S,11S,12S)-2,6-di-*tert*-butyl-9,10-dihydro-9,10-ethanoanthracene-11,12-dicarboxylate (1) at the gram scale. The purity and stereochemistry of 1 was checked by HPTLC and its optical activity ($[\alpha]_D^{20} = -53.3°$), for which Kräutler et al.[15] reported an *ee* of >99.9%. This is very

important, because a racemization in the following five reaction steps is impossible. Stereochemically pure dicarboxylate **1** was transferred in a four-step synthesis (saponification, decarboxylation, oxidation (OsO₄), Swern oxidation) to stereochemically pure (9S,10S)-1,2-diketone **5** (Scheme 2). The oxidative decarboxylation with lead(IV) acetate and copper(II) acetate in a mixture of dry pyridine and dry toluene[16] to olefin **3** (1.50 g of **2** react to 343 mg of **3**) is the limiting factor of the synthetic route, because any attempts to scale up this reaction step led to dramatic losses in yield. The spectra of diketone **5** indicate its C_2 symmetry (¹H NMR: 5 signals, Figure 1; ¹³C NMR: 10 signals, see the Supporting Information). The oxidation of the diols to the diketone is also proven by the carbonyl signal at $\delta = 184.1$ ppm and the carbonyl band (1738 cm⁻¹) in the infrared spectrum.
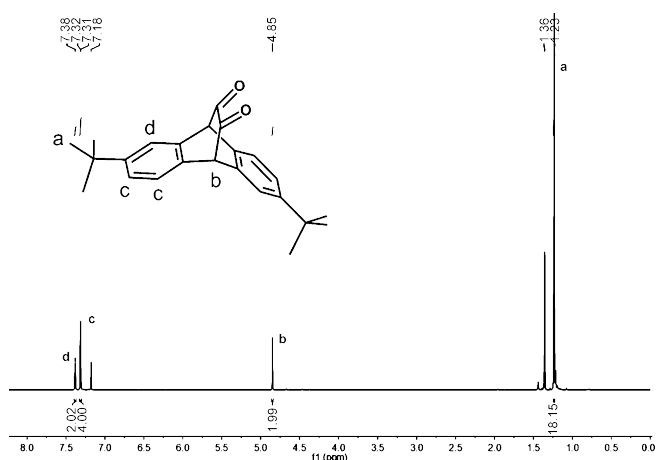

Figure 1. ¹H NMR spectrum of diketone **5**; solvent: CDCl₃; signal at 1.33: cyclohexane.

In the final step, the chiral receptor **7** was obtained by the condensation of diketone **5** with hexaaminotetramethyltribenzotriquinacene (**6**)[17] in chloroform with a catalytic amount of trifluoroacetic acid combined with water trapping (Scheme 2, e). The symmetry of the diketone **5** has a decisive influence on the reaction. Only stereochemically pure (2S,7S,16S,21S,30S,35S)-**7** can be formed in this reaction if stereochemically pure S,S diketone **5** is used, because of its C_2 symmetry eliminating the necessity of the separation of stereoisomers (Scheme 3). Nevertheless, receptor **7** had to be purified by column chromatography. To avoid difficult-to-separate byproducts due to incomplete condensation, a 2:1 excess of diketone **5** was used in the reaction. This decreases the yield of the product from theoretically 100 to 69%.

Kuck et al. previously published the synthesis of several C_3 symmetric tribenzotriquinacenes. In some cases the enantiomers were not isolated, because an unexpected supramolecular cubic compound crystallized from the racemic mixture[18] or the separation was not necessary.[19] In yet another case the enantiomers were successfully separated through the conversion of the pair of enantiomers into diastereomers followed by several chromatographic purification steps.[20]
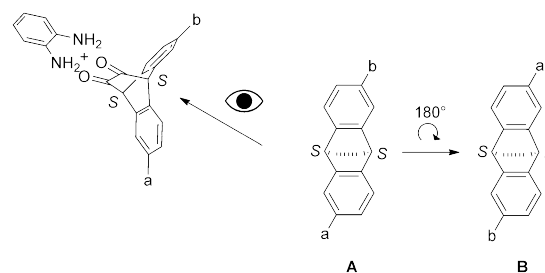
Scheme 3. Schematic drawing of the condensation reaction of one side arm of **6** with diketone **5** (a and b are *tert*-butyl-groups, so the products A and B are identical).

The structure of host **7** was verified by ¹H and ¹³C NMR spectroscopy, mass spectrometry and single crystal X-ray structure analysis.

The NMR spectra of **7** (¹H, Figure 2 and ¹³C, see the Supporting Information) clearly confirm the C_3 symmetry of the molecule (¹H NMR: 14 signals; ¹³C NMR: 27 signals). Note that the aromatic rings that are annelated at the 2.2.2-bicyclooctane moiety are not chemically equivalent. This was also observed in similar tribenzotriquinacene-based host systems.[12–14] A more detailed assignment of the NMR signals is given in the Supporting Information. The molecular mass of receptor **7** ($M_r = 1358.2$ u) was confirmed by MALDI and ESI mass spectrometry.
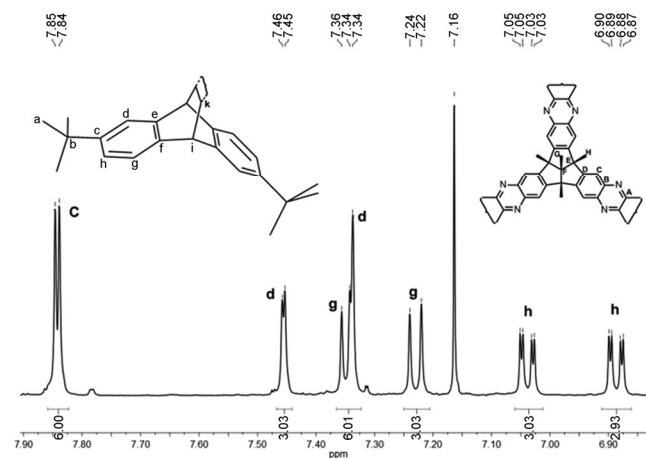

Figure 2. Aromatic region of the ¹H NMR spectrum of receptor **7** and the assignment of the corresponding signals.

Single crystal X-ray structure analysis of 7·2 C₂H₅OH·o-C₆H₄Cl₂

Yellow single crystals of **7·2 C₂H₅OH·o-C₆H₄Cl₂** were obtained after several days at room temperature upon slow diffusion of ethanol into a 1,2-dichlorobenzene solution of **7**. The chiral receptor **7** crystallizes in the orthorhombic crystal system, in space group $P2_12_12_1$ (no. 19) with lattice parameters of $a = 17.5092(15)$, $b = 21.167(2)$, $c = 23.599(2)$ Å, and a volume of the unit cell of $V = 8746.2(1)$ Å³. Assuming that the carbon atom placed on the threefold axis represents the origin of a Cartesian

coordinate system, the three vectors from this central bridge-head carbon atom pointing towards the centroids of the phen-azine rings form dihedral angles of 80.0 and 82.4°, respectively. The center-to-center distances between the centroids of the aromatic rings of the upper rim side of the molecule range from 8.83 to 11.91 Å, which indicates considerable deviation of **7·2C₂H₅OH·o-C₆H₄Cl₂** from the expected and NMR spectrosco-py confirmed (see above) perfect molecular symmetry of **7** (Figure 3a). These values slightly differ from the distances ob-served in $C_{60}⊂C_{98}H_{96}N_6O_{12}$·$3C_7H_8$ ($C_{60}⊂$tribenzotriquinacene complex·3toluene) 11.77–11.83 Å, and angles of 89.0–89.5°, in which the peripheral benzene rings define an almost perfect set of axes for a Cartesian coordinate system (Figure 3a, gray vectors).[12] The packing diagram of **7** is shown in Figure 3c. The crystal structure of **7·2C₂H₅OH·o-C₆H₄Cl₂** consists of recep-tor molecules **7**, which are interlocked with one another; one of the *tert*-butyl groups is directed into the center of the adja-cent receptor molecule. This *tert*-butyl group lies almost paral-lel along to the crystallographic 2₁-screw axis. Additionally, one of the *tert*-butyl groups of **7** is also rotationally disordered. Fur-ther details of the crystallographic data collection and analysis of **7** are given in the Experimental Section.

In the crystal lattice disordered solvent molecules (EtOH and 1,2-dichlorobenzene) are located in the void space between the packed receptor molecules. The total solvent-filled space of the unit cell of **7·2C₂H₅OH·o-C₆H₄Cl₂** amounts to 1846.8 Å³

per unit cell volume 8746.2 Å³ (21.1%). The high content of rel-atively volatile solvent molecules and the fact that all mole-cules in the crystal lattice merely interact via weak intermolec-ular forces (van der Waals and π–π interactions) provides an explanation for the observed solvent disorder, diminishing the quality of the experimentally available X-ray data set. A reliable determination of the absolute configuration of huge organic molecules, such as **7** normally requires data sets of high quality and the presence of heavy atom scatterers.[21] However, since the absolute configuration of the chirality inducing synthon (diketone **5**) is known, it was possible to derive the correct ab-solute all-*S* configuration of the final product **7**. This was par-tially confirmed by refinement of the structure and by keeping track of the Flack parameter,[21] which was refined to 0.03(5). For checking the refinement correctness, the structure was in-verted and the Flack parameter was equal to 0.8(2).

Still, to strengthen the conclusion concerning the stereo-chemistry, the absolute configuration of **7** was confirmed inde-pendently from the X-ray crystallographic results through vi-brational circular dichroism (VCD) and electronic circular di-chroism (ECD) spectroscopic measurements, which provided unequivocal evidence for the suggested stereochemistry of **7**.

Chiroptical spectroscopy

VCD and ECD spectra were recorded, establishing the chiral nature and the absolute configuration of **7**. VCD and ECD allow the establishment of the absolute configuration (AC) of a compound by comparison to an ab initio computed spec-trum for a known absolute configuration. VCD has the advant-age that, compared to ECD, it is more widely applicable for both stereocenter-related chirality as well as noncentral chirali-ty.[22]

When assigning the absolute configuration of a molecule using VCD, the first step is always to check whether the experi-mental and computed IR spectra are sufficiently similar (see Computational Section for details). Both the computed and ex-perimental IR spectrum of the receptor **7** are shown in Figure 4.

Figure 4 clearly shows excellent agreement between both spectra with a near perfect one-to-one correspondence. In some cases, neighboring peaks in one spectrum may occasion-ally become shoulders of peaks in the other but this is also in
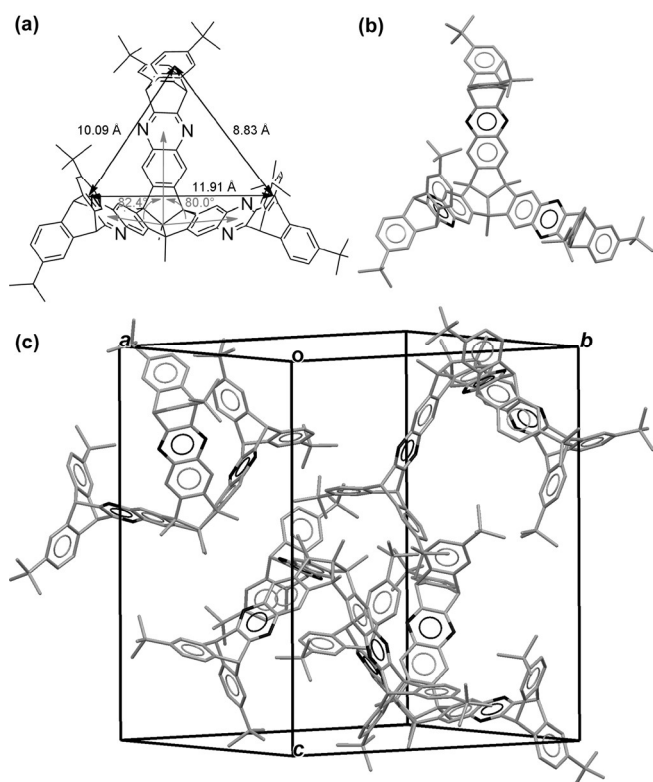

Figure 3. a) Molecular structure and absolute configuration of **7**. b) View along the C_3 axis into the center of the cavity of receptor **7**. c) Packing dia-gram of receptor **7·2C₂H₅OH·o-C₆H₄Cl₂**. Solvent molecules and hydrogen atoms have been omitted for clarity. For disordered *tert*-butyl substituents only one rotamer is shown.
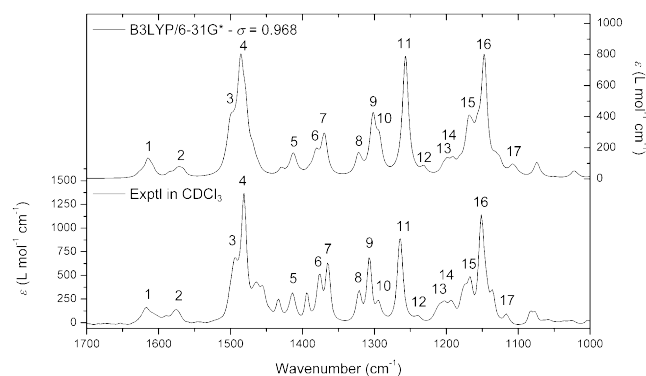

Figure 4. Computed B3LYP/6-31G* and experimental CDCl₃ IR spectra of **7**.

part due to natural and instrumental line broadening and the Lorentzian broadening performed for the calculated spectrum. The excellent agreement in the IR spectrum allows for a manual assignment of the VCD peaks. The computed and experimental VCD spectra are shown in Figure 5.
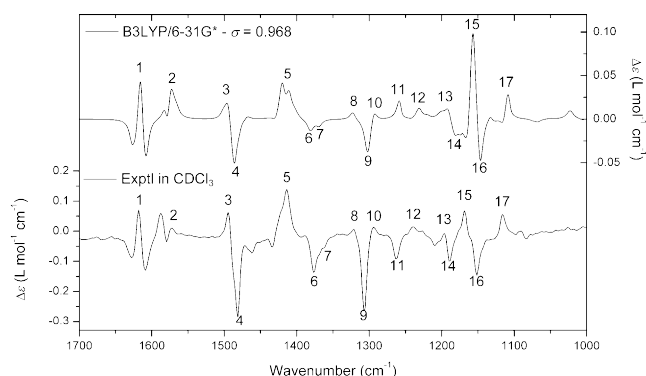

Figure 5. Computed B3LYP/6-31G* and experimental CDCl$_3$ VCD spectra of **7**.

The agreement between both VCD spectra is excellent and the stereochemistry of the experimental sample thus corresponds to (2S,7S,16S,21S,30S,35S)-**7**. Only near 1260 cm^{-1} a less-good correspondence is found, possibly due to the experimental broadening and the Lorentzian broadening.

We also measured the ECD spectrum and found the agreement with the computed spectrum somewhat less good than that for the VCD spectrum.

The two spectra are similar but do not match to the same degree as the VCD spectra as shown in Figure 6. The most important effect occurs around 220 nm and is present in both spectra. Other features are either a shoulder of the peak around 230 nm or are less prominent. Yet, there appears a fairly good correspondence between both spectra. Taken together, VCD is clearly better than ECD when it comes to establishing the absolute configuration using computed reference
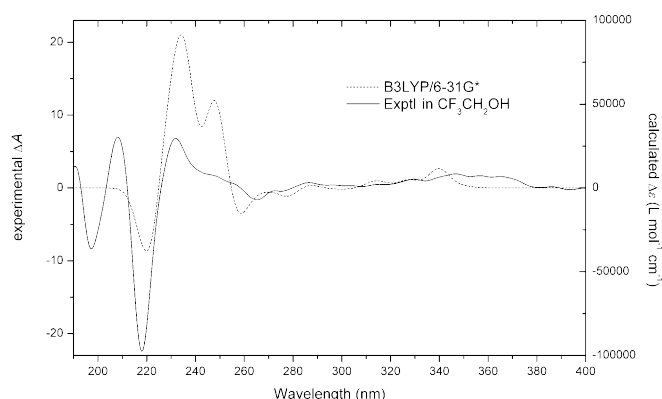

Figure 6. Experimental and computed B3LYP/6-31G* ECD spectrum of **7**. The experimental spectrum was obtained using 2,2,2-trifluoroethanol as solvent. A liquid cell with an optical path length of 1 mm was used. Due to the low solubility and limited amount of **7** being dissolved, no exact concentration could be established.

spectra. The reason for this is that VCD is much more information-rich as there are more vibrational transitions than important electronic transitions and the latter are moreover harder to compute accurately.

Host–guest complex formation

The stoichiometry of host–guest complexes formed between receptor **7** and C$_{60}$ (between **7** and **R** (Figure 7), respectively) and the quantitative host–guest association constants were determined by UV/Vis spectroscopic titration experiments. Unfortunately, **7** is not soluble in the typical solvents for these kinds of investigations (benzene or toluene), so we used a solvent mixture of CHCl$_3$ and CS$_2$, which we used in previous studies;[12–14] this allowed us to compare the results from these studies with the corresponding values from our previous investigations on similar [C$_{60}$⊂tribenzotriquinacene] complexes.
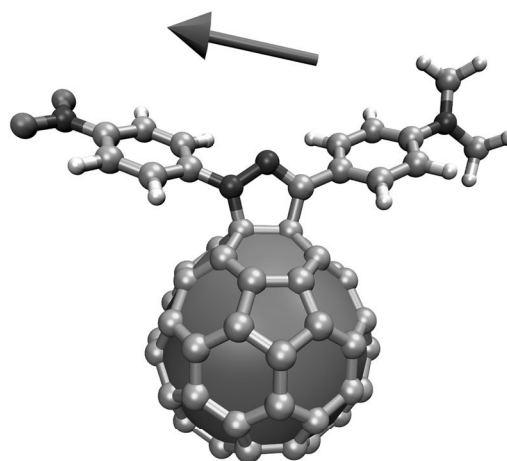

Figure 7. Optimized structure (B3LYP/cc-pVDZ) of **R** (1'-(4-nitrophenyl)-3'-(4-N,N-dimethylaminophenyl)-pyrazolino[4',5':1,2][60]fullerene),[10] a fullerene rotor augmented by a dipolar substituent. The arrow indicates the direction of the computed dipole moment of 8.6 D.

In a first experiment nine solutions of host **7** and C$_{60}$ mixed at mole fractions of 0.1 to 0.9 at 10^{-4} mol L^{-1} were prepared and their UV/Vis spectra were measured. To our surprise no complex formation could be determined, but in previous investigations[14] it was found that self-aggregation of host molecules has a large influence on complex formation. By using the mild electrospray ionization technique we were able to detect the dimer of receptor **7**.

A comparison of the isotope pattern of the ESI mass spectrum with the calculated ones of the monomer ((C$_{98}$H$_{96}$N$_6$)$^+$) and the dimer ((C$_{98}$H$_{96}$N$_6$)$_2^{2+}$) shows that receptor **7** dimerizes in the gas phase to a certain extent (Figure 8).

To take the experimental artefacts of nonspecific complex formation,[24] such as nonlinearity[25] or self-aggregation,[26] into account, the validity of the Lambert–Beer law, that is, a linear dependence of absorbance from the solute's concentration, was tested for pure solutions of host **7** in the appropriate concentration regime within a first set of experiments. Surprisingly
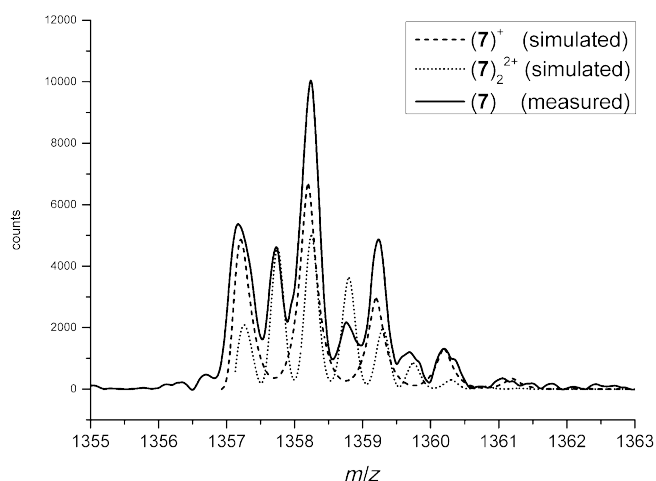
Figure 8. Partial enlargement of the ESI mass spectrum of receptor **7**. Isotope patterns of **7** (solid line: measured by ESI-MS, dotted line: calculated[23] for $(C_{98}H_{96}N_6)^+$, dashed line: calculated for $(C_{98}H_{96}N_6)_2^{2+}$).

no such artefacts were detectable (Figure S22 in the Supporting Information).

This result might point to the fact that dissociation of the dimer does not occur at room temperature but requires higher temperatures. Because of this we stored the mixtures of host **7** and C_{60} for 72 h at 60 °C in tightly sealed vessels for the following experiments. Subsequently, Job plot investigations (method of continuous variation)[27] showed a 1:1 binding stoichiometry between host **7** and C_{60} (Figure 9, top).

The quantitative association constant was determined by the procedure outlined by Conners.[28] For this purpose the changes of the absorbance were plotted against the host concentration, and the individual association constant was fitted by a nonlinear regression (see Formula S2 in the Supporting Information; Figure 9, bottom) leading to an equilibrium constant of $K_1 = 319(\pm156)$ M^{-1}. This is an averaged value from four independent UV/Vis titration experiments (Table S1 in the Supporting Information; for all curve regressions see Figure S2 in the Supporting Information). In a similar experiment an equilibrium constant of $K_1 = 110(\pm50)$ M^{-1} for the 1:1 complex [R⊂**7**] was determined (Table S2 and Figure S4 in the Supporting Information).

This low association constant value in the present study is consistent with our earlier findings for the first generation hosts **8a/b** (**8**, $K_1 = 2908(\pm360)$ M^{-1}, Figure 10) and the second generation host **10** ($K_1 = 14550(\pm867)$ M^{-1}, Figure 10). Kuck et al. presented a fullerene (C_{60}) host–guest system based on a conformationally rigid tribenzotriquinacene derivative with a comparable association constant (compound **9**,[29] $K_1 = 321$ M^{-1}, Figure 10), but in this system the concave binding pocket shows a poorer shape complementarity towards C_{60} compared to that in hosts **8a/b**, **10** and receptor **7**. However, the equilibrium constant of **7** is in good agreement with the third generation host **11** ($K_1 = 213(\pm37)$ M^{-1}). In the case of **8** and **10**, the cavities are freely accessible for guests and no conformational change is necessary. In contrast, the cage of host **11** in its native form is blocked from above and is only accessi-
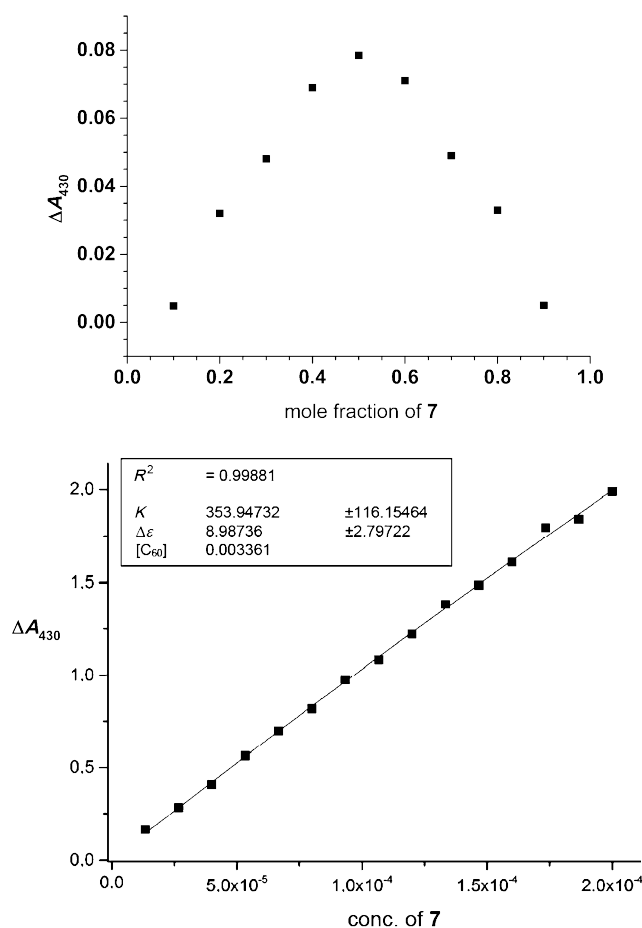

Figure 9. Job plot showing the 1:1 stoichiometry of host C_{60}⊂**7** in $CHCl_3/CS_2$ (1:1) at 10^{-4} $mol\,L^{-1}$ (top). Exemplary nonlinear curve regression of a titration of C_{60} (3.361×10^{-3} $mol\,L^{-1}$) with host **7** (bottom).

ble for C_{60} through the side-portals. Both the deformation of the arms upon uptake of C_{60} and the loss of entropy hamper the complexation and reduce the equilibrium constant. In addition, as well as for **7**, the formation of dimers $(11)_2$, was detected by MALDI mass spectrometry, reducing the amount of free receptor.[14]

Molecular dynamics simulations

Following previous work,[13,14] we investigated the host–guest interaction of the chiral receptor **7** with the dipolar rotor **R** by means of force-field-based molecular simulations. The first principles derived force field (MOF-FF)[30] has been parameterized for receptor **8a**, **10** and **11**,[14] and was easily extended to also describe **7**. Accordingly, a parameterization for the dipolar substituent of **R** was generated. For this purpose **R** and slightly reduced models thereof were optimized on the B3LYP/cc-pVDZ level of theory. Atomic charges were derived by a Merz–Kollmann (MK) sampling of the electrostatic potential. Both the optimized structure and the computed Hessian matrix of second derivatives were used as reference data for the genetic-algorithm-based optimization of force field parameters. For details see ref. [30].
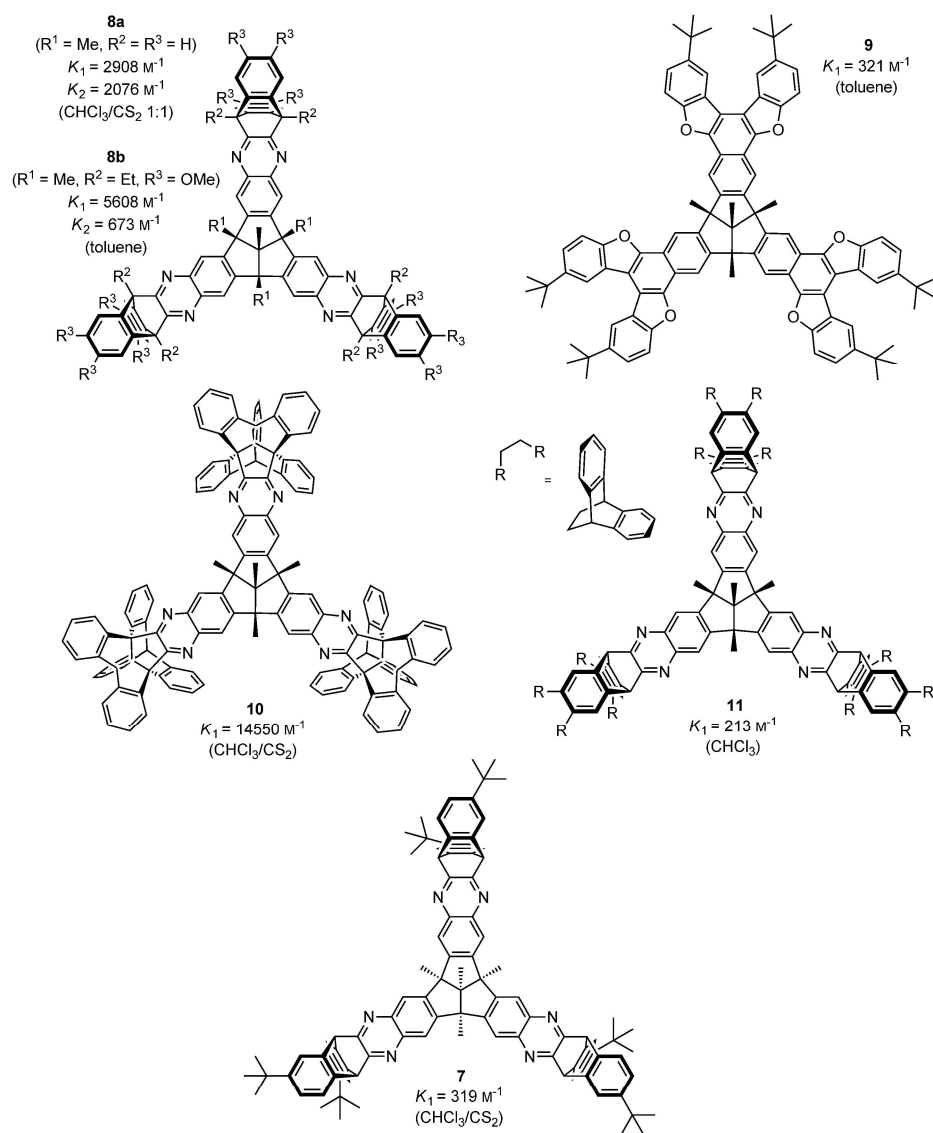
8a
(R^1 = Me, R^2 = R^3 = H)
K_1 = 2908 M^{-1}
K_2 = 2076 M^{-1}
($CHCl_3/CS_2$ 1:1)

8b
(R^1 = Me, R^2 = Et, R^3 = OMe)
K_1 = 5608 M^{-1}
K_2 = 673 M^{-1}
(toluene)

9
K_1 = 321 M^{-1}
(toluene)

10
K_1 = 14550 M^{-1}
($CHCl_3/CS_2$)

11
K_1 = 213 M^{-1}
($CHCl_3$)

7
K_1 = 319 M^{-1}
($CHCl_3/CS_2$)

Figure 10. Summary of tribenzotriquinacene-based receptor molecules that form host–guest complexes with fullerene C_{60} and their experimental association constants.[12–14,29]

whereas in solvated state, dispersive interactions of the dipolar group with the solvent may well compensate the effect. In addition, the upright form can be expected to be entropically preferred and, last but not least, by a field-driven rotation also the electric field perpendicular to the C_3 axis essentially stabilizes the upright configuration. In a preliminary test we immersed the host–guest complex into a box of 500 explicit benzene molecules (using periodic boundary conditions). In a short MD simulation at constant temperature of 300 K the trajectory indeed showed primarily upright configurations. It can be concluded that under realistic conditions the system is suitable for a rotational motion with the rotors axle, defined by the dipolar group, staying perpendicular to the C_3 symmetry axis of the receptor. In order to mimic this behavior also in case of the gas-phase simulations we added a soft harmonic angle restraint between the central carbon of the receptor, the center of mass of the C_{60} fragment and the top nitrogen atom of the rotor in order to maintain the rotor in an upright position.

In the next step we used a strict dihedral constraint to enforce a stepwise rotation of the dipolar rotor with respect to the receptor. Again, primarily because of the rotational freedom of the *tert*-butyl groups, for each rotational position of the rotor numerous local minima exist on the potential energy surface. Thus, in order to give a faithful representation of the energetics of rotation we have sampled each position between 0° to 120° (because of the threefold symmetry) in steps of 1° with

In order to keep the numerical effort tractable we treated the complex of **R** in **7** in the absence of a solvent. From a series of short molecular dynamics (MD) sequences and consecutive energy minimizations it is clear that, due to the free rotation of the *tert*-butyl substituents of the receptor as well as rotational degrees of freedom in the dipolar group of **R**, multiple local minima exist for this system. Most importantly, in the gas phase the system is dominated by multiple low energy conformations, where the dipolar group is nested in a pocket between the three arms of the receptor as shown in Figure 11 a. Configurations like in Figure 11 b are about 13 kcal mol^{-1} higher in energy. It is clear that such a tilted low energy conformation would likely prevent any rotational motion around the C_3 symmetry axis of the rotor. However, low energy tilted conformations are mainly stabilized by dispersive interactions between the dipolar group (π–π interactions) and the receptor arms. This stabilization is present only in the gas phase,
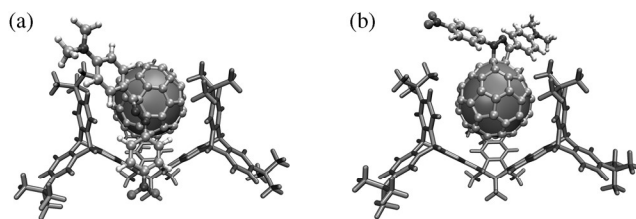

Figure 11. Force-field optimized local energy minima of the host–guest complex of **7** and **R**: a) low-energy conformation; b) upright conformation.

a short NVT simulation of 0.3 ns and averaged the force field strain energy. The result is shown in a scatter plot in Figure 12. It clearly shows an asymmetric profile as expected for the chiral receptor, with a steeper flank on the left and a slight dip to the right of the maximum. Three representative snapshots of the structure as a top view are shown as insets for the maximum, the minimum and the second, higher-lying minimum. However, the barrier is with about 1.5 kcal mol^{-1} rather small and the amount of asymmetry in the profile is not very pro-
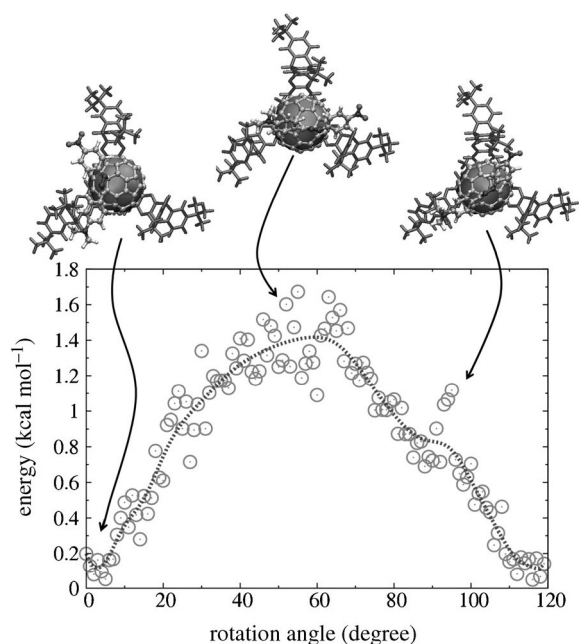

Figure 12. Rotational energy profile for a 120° rotation of the dipolar rotor from averages of strain energies over short MD simulation trajectories indicating the asymmetric profile due to the chirality of the receptor.

nounced with respect to the statistic scatter of the energies. This indicates that the strain interactions with the dipolar group of the rotor are not very strong, which is beneficial for a facile rotation on the one side, but also limits the amount of asymmetry, necessary for an unidirectional ratchet-like rotation. The structural reason for this is the fact that the *tert*-butyl groups do not extend much over the "rim" of the receptor and for a perfectly upright position of the rotor (Figure 11 b) the steric interaction gets small. Nevertheless, because of this asymmetric rotational profile, it is in principle possible to, for example, drive a unidirectional rotation by coupling to an oscillating electric field. Molecular dynamics investigations including solvation effects of this system and derivatives thereof are currently underway, but are beyond the scope of the current study.

Conclusion

A first chiral tribenzotriquinacene C_{60} receptor **7** has been synthesized and its absolute configuration has been determined by VCD and ECD spectroscopy. The structure of **7** was con-

firmed by ^{1}H and ^{13}C NMR spectroscopy and mass spectrometry as well as by single crystal X-ray diffraction. We show that this host leads exclusively to the formation of 1:1 complexes with C_{60} and the fullerene-based dipolar rotor **R**. The resulting moderate K_1 values of 319 and 110 M^{-1} for the association constants of [$C_{60} \subset$ **7**] and [R$\subset$**7**], respectively, are in good agreement with the results of our previous investigations.[12–14] The functionalized upper rim of host **7** prevents the formation of 1:2 complexes but the functional groups of two host molecules are able to get entangled with each other, which results in the formation of stable dimers (**7**)$_2$ and consequently leads to small K_1 values. Additionally the sterical hindrance of the functional groups inhibits the formation of stable complexes with C_{60}-based guest molecules possessing bulky substituents.

Molecular dynamics simulations of [R$\subset$**7**] reveal an asymmetrical rotational barrier, which might help unidirectional rotational motion if the device is operated under the appropriate experimental conditions. In addition, the calculations show that the gas phase global minimum with the rotor nested between the arms of the receptor will be destabilized by solvation and a preference for the proper upright position of the rotor, which allows rotational motion, can be expected under experimental conditions.

To optimize the function of tribenzotriquinacenes as stators for unidirectional ratchets, the design of the chiral stator should be slightly modified to obtain larger K_1 values. A good option could be to transfer the chiral design of **7** to the centrohexaindane-extended receptor **10** (Figure 10), which has a huge K_1 value (14550 M^{-1}) for the 1:1 complex with C_{60}. However, enhancing shape complementarity between rotor and stator does not always and automatically lead to the desired enhancement in device stability, which in turn is a necessary requirement for device self-assembly. Adding complementary electric charges to the rotor and the stator, respectively, might be a suitable route towards improved nanoratchet designs. If and how these charges might interfere with operating the device by alternating electric fields will be subject of future studies.

Experimental Section

General

Melting points: Optimelt, MPA100. Infrared (IR) spectra: Bruker, Equinox 55 with ATR unit. NMR spectroscopy: Bruker Avance 400 or Mercury plus 400 high-resolution system (Fa. Varian Deutschland GmbH). ^{1}H NMR (400 MHz) and ^{13}C NMR (100 MHz) chemical shifts are given in ppm relative to the solvent signal. EI mass spectra: Finnigan MAT, SSQ 7000 mass spectrometer, single-stage-quadrupol system, intensities relative to base peak. MALDI-TOF mass spectra: Bruker Daltonics REFLEX III. N$_2$-laser (337 nm), pulsed ion extraction (PIE), HIMAS-detector, acceleration voltage 20 kV, matrix: DHB. ESI mass spectrometry was performed on a Varian LC-MS 500 (50–2000 Da) using isopropanol as solvent. The optical activity was measured by an Anton Paar MCP 500 polarimeter. Elemental analysis: Vario EL III, Elementar-Analysensysteme GmbH. Thin layer chromatography: silica gel F$_{254}$ on Al foil (Merck). Gravity column chromatography: (Silica gel 60, ∅ = 0.063–0.200 mm, Merck). All commercially available reagents and solvents were used without fur-

ther purification. Dry solvents were purchased from Sigma–Aldrich®. Di[(1R)-menthyl] (9S,10S,11S,12S)-2,6-di-tert-butyl-9,10-di-hydro-9,10-ethanoanthracene-11,12-dicarboxylate (**1**) was synthesized from (−)dimenthyl fumarate[31] and 2,6-di-tert-butylanthracene[32] according to the literature,[15] as well as hexaaminotetrame-thyltribenzotriquinacene (**6**).[17] The purity and stereochemistry of **1** was controlled by high-performance thin layer chromatography (Silica gel 60 RP-18 F254s on Al foil (Merck), eluent: MeOH) and its optical activity ([α]$_D^{20}$ = −53.3).

Synthesis and characterization

(9S,10S,11S,12S)-2,6-Di-tert-butyl-9,10-dihydro-9,10-ethanoan-thracene-11,12-dicarboxylic acid (2): An aqueous solution of NaOH (2.86 g; 71.4 mmol) in H_2O (50 mL) was slowly added to a re-fluxing solution of diester[15] **1** (5.1 g, 7.50 mmol) in EtOH (350 mL). The resulting clear solution was refluxed for three days. The etha-nol was evaporated on a rotary evaporator, H_2O (150 mL) was added to the residue and the mixture was extracted three times with n-hexane (150 mL) to remove (−)menthol. The aqueous solu-tion was cooled to 0 °C in an ice bath and acidified with conc. HCl (pH∼2). The precipitated white solid was filtered by suction, washed with water and dried in vacuum to obtain dicarboxylic acid **2** (2.58 g, 6.35 mmol, 85%). M.p.: 197 °C dec.; ^{1}H NMR (400 MHz, [D$_8$]THF): δ = 7.55 (d, ^{2}J(H,H) = 2.00 Hz, 2H), 7.32 (d, ^{3}J(H,H) = 8.09 Hz, 2H), 7.24 (dd, ^{3}J(H,H) = 8.09 Hz, ^{4}J(H,H) = 2.00 Hz, 2H), 4.84 (s, 2H), 3.41 (s, 2H), 1.45 ppm (s, 18H); ^{13}C NMR (100 MHz, [D$_6$]DMSO): δ = 173.4 (q), 148.4 (q), 142.9 (q), 137.7 (q), 124.2 (t), 122.2 (t), 120.2 (t), 47.9 (t), 45.9 (t), 34.3 (q), 31.3 ppm (p); IR (ATR): $\tilde{v}$ = 2960, 2905, 2869, 1706, 1485, 1416, 1363, 1264, 1174, 884, 834, 617 cm^{-1}; MS (70 eV): m/z (%): 406 (17) [M$^+$], 290 (100), 275 (41), 219 (16); elemental analysis calcd (%) for C$_{26}$H$_{30}$O$_4$: C 76.82, H 7.44; found: C 76.54, H 7.51.

(9S,10S)-2,6-Di-tert-butyl-9,10-dihydro-9,10-ethenoanthracen (3): A solution of dicarboxylic acid **2** (1.50 g, 3.69 mmol) in a mixture of anhydrous pyridine (4 mL) and anhydrous toluene (75 mL) was heated to 100 °C. Cu(OAc)$_2$ (800 mg, 4.00 mmol) and Pb(OAc)$_4$ (3.60 g, 812 mmol) were added and the mixture was refluxed for 45 min. The hot solution was filtered through a pad of celite and the solvent was evaporated. The crude product was purified by column chromatography on silica (n-hexane/diethyl ether 9:1) to give olefin **3** (343 mg, 1.08 mmol, 29%) which contains 5–15% 2,6-di-tert-butylanthracene. Analytically pure product was obtained as a colorless solid by additional column chromatography on silica (cyclohexane). M.p.: 169–171 °C; ^{1}H NMR (400 MHz, CDCl$_3$): δ = 7.23 (d, ^{2}J(H,H) = 2.00 Hz, 2H), 7.10 (d, ^{3}J(H,H) = 7.58 Hz, 2H), 6.90 (dd, ^{3}J(H,H) = 3.54 Hz, ^{4}J(H,H) = 3.03 Hz, 2H), 6.86 (dd, ^{3}J(H,H) = 7.58 Hz, ^{4}J(H,H) = 2.00 Hz, 2H), 4.98 (dd, ^{3}J(H,H) = 3.54 Hz, ^{4}J(H,H) = 3.03 Hz, 2H), 1.19 ppm (s, 18H); ^{13}C NMR (100 MHz, CDCl$_3$): δ = 147.4 (q), 146.2 (q), 143.4 (q), 139.8 (q), 122.3 (t), 120.8 (t), 120.4 (t), 51.2 (t), 34.5 (q), 31.6 ppm (p); IR (ATR): $\tilde{v}$ = 2954, 2864, 1477, 1361, 1262, 830, 801, 693, 667, 570, 542 cm^{-1}; MS (70 eV): m/z (%): 316 (81) [M$^+$], 301 (51), 259 (100), 203 (33); elemental analysis calcd (%) for C$_{24}$H$_{28}$: C 91.08, H 8.92; found: C 90.96, H 8.90.

(9S,10S,11R,12S)- and (9S,10S,11S,12R)-2,6-Di-tert-butyl-9,10-di-hydro-9,10-ethanoanthracene-11,12-diol (4): Under nitrogen, osmium tetroxide (2.18 mL, 2.5 wt% in tBuOH) was added to a solu-tion of 4-methylmorpholine-4-oxide (1.10 mL, 50 wt% in H_2O, 4.67 mmol) in acetone (100 mL). After being stirred for 10 min a so-lution of olefin **3** (343 mg, 1.08 mmol) in acetone (25 mL) was added. After being stirred for 15 h at RT the reaction was quenched by adding a solution of sodium dithionite (900 mg, 5.18 mmol) in water (3 mL). The mixture was stirred for 10 min and

subsequently filtered through a pad of celite. The solvent was evaporated and the crude product was purified by column chro-matography on silica (gradient: 1, n-hexane/diethyl ether 9:1; 2, cy-clohexane/ethyl acetate 4:1; 3, cyclohexane/ethyl acetate 4:1) to give diol **4** (236 mg, 673 μmol, 62%) as a colorless solid. M.p.: 255–257 °C; ^{1}H NMR (400 MHz, CDCl$_3$): δ = 7.28 (d, ^{4}J(H,H) = 2.02 Hz, 1H), 7.22 (d, ^{4}J(H,H) = 2.02 Hz, 1H), 7.20 (d, ^{3}J(H,H) = 7.58 Hz, 1H), 7.14 (d, ^{3}J(H,H) = 7.58 Hz, 1H), 7.12 (dd, ^{3}J(H,H) = 7.58 Hz, ^{4}J(H,H) = 2.02 Hz, 1H), 7.06 (dd, ^{3}J(H,H) = 7.58 Hz, ^{4}J(H,H) = 2.02 Hz, 1H), 4.256 (s, 1H), 4.251 (s, 1H), 3.92 (m, 2H), 2.07 (d, ^{3}J(H,H) = 6.06 Hz, 1H), 2.02 (d, ^{3}J(H,H) = 6.57 Hz, 1H), 1.20 (s, 9H), 1.19 ppm (s, 9H); ^{13}C NMR (100 MHz, CDCl$_3$): δ = 149.8 (q), 149.7 (q), 139.8 (q), 138.4 (q), 137.1 (q), 135.7 (q), 126.0 (t), 124.2 (t), 123.7 (t), 123.5 (t), 123.4 (t), 121.9 (t), 68.41 (p), 68.36 (p), 51.20 (p), 51.17 (p), 34.6 (q), 31.55 (p), 31.52 ppm (p); IR (ATR): $\tilde{v}$ = 3351$_{br}$, 2955, 2865, 1484, 1362, 1264, 1064, 1001, 831, 805, 588, 544 cm^{-1}; MS (70 eV): m/z (%): 319 (43) [M$^+$−H_2O−H_3CO], 290 (100) [M$^+$−2H_2CO]; elemental analysis calcd (%) for C$_{24}$H$_{30}$O$_2$: C 82.24, H 8.63; found: C 82.03, H 8.52.

(9S,10S)-2,6-Di-tert-butyl-9,10-dihydro-9,10-ethanoanthracene-11,12-dione (5): Under nitrogen trifluoroacetic acid anhydride (0.32 mL, 2.1 mmol) was added at −78 °C to a mixture of anhy-drous DMSO (0.2 mL, 0.25 mmol) and anhydrous CH_2Cl_2 (12 mL) and the resulting solution was stirred for 10 min. A solution of diol **4** (260 mg, 740 μmol) in CH_2Cl_2/DMSO (2:1; 3 mL) was added within 15 min and the mixture was stirred an additional 60 min at −78 °C. Triethylamine (0.7 mL, 5.0 mmol) was added slowly; the re-action mixture was allowed to warm to 5 °C and poured subse-quently into 2 M HCl (25 mL). When the evolution of gas had stopped, the two layers were separated. The aqueous layer was ex-tracted six times with CH_2Cl_2. The combined organic layers were washed with water (6×) and dried with sodium sulfate. The solvent was evaporated and the crude product was purified by column chromatography (cyclohexane/ethyl acetate 1:1) to yield dion **5** (250 mg, 722 μmol, 98%) as a yellow powder. M.p.: 213 °C; ^{1}H NMR (400 MHz, CDCl$_3$): δ = 7.36 (s, 2H), 7.298 (s, 2H), 7.295 (s, 2H), 4.83 (s, 2H), 1.22 ppm (s, 18H); ^{13}C NMR (100 MHz, CDCl$_3$): δ = 184.1 (q), 153.1 (q), 134.8 (q), 132.0 (q), 126.4 (t), 125.9 (t), 123.2 (t), 59.9 (t), 34.9 (q), 31.3 ppm (p); IR (ATR): $\tilde{v}$ = 2962, 2864, 2832, 1738, 1479, 1460, 1431, 1363, 1264, 1112, 931, 891, 833, 699, 623, 503 cm^{-1}; MS (70 eV): m/z (%): 290 (100); elemental analysis: calcd (%) for C$_{24}$H$_{26}$O$_2$: C 83.20, H 7.56; found: C 82.96, H 7.42.

(2S,7S,16S,21S,30S,35S)-4,10,18,24,32,38-Hexa-tert-butyl-13b,27b,41b,41d-tetramethyl-13b,27b,41b,41d-tetrahydro{1″,4″-diaza-9″,10″-dihydro-9″,10″-o-benzoanthraceno}[2″,3″:5′,6′]inde-no[1′,2′,3′:3,4]{6′,11′-diaza-5′,12′-dihydro-5′,12′[1″,2″]benzo-naphthaceno}[8′,9′:5,6]pentaleno[1,2-k]{6′,11′-diaza-5′,12′-dihy-dro-5′,12′[1″,2″]benzonaphthacene} (7): A solution of hexaamino-tetramethyltribenzotriquinacene **10**[17] (220 mg, 635 μmol), dike-tone **5** (45 mg, 106 μmol) and a catalytic amount of trifluoroacetic acid in anhydrous chloroform (50 mL) was refluxed under argon and water separation for 48 h. The solvent was removed and the residue was purified by column chromatography (chloroform) to yield host **11** (100 mg, 74 μmol, 69%) as a light yellow solid. M.p.: >400 °C; ^{1}H NMR (400 MHz, CDCl$_3$): δ = 7.85 (s, 3H), 7.84 (s, 3H), 7.45 (d, ^{4}J(H,H) = 1.52 Hz, 3H), 7.34 (d, ^{3}J(H,H) = 7.58 Hz, 3H), 7.33 (d, ^{4}J(H,H) = 2.02 Hz, 3H), 7.23 (d, ^{3}J(H,H) = 8.08 Hz, 3H), 7.04 (dd, ^{3}J(H,H) = 8.08 Hz, ^{4}J(H,H) = 2.02 Hz, 3H), 6.88 (dd, ^{3}J(H,H) = 7.58 Hz, ^{4}J(H,H) = 1.52 Hz, 3H), 5.36 (s, 6H), 1.68 (s, 9H), 1.30 (s, 3H), 1.17 (s, 27H), 1.07 ppm (s, 27); ^{13}C NMR (100 MHz, CDCl$_3$): δ = 157.21 (q), 157.19 (q), 151.06 (q), 151.04 (q), 149.8 (q), 149.7 (q), 141.8 (q), 141.7 (q), 139.4 (q), 139.0 (q), 138.9 (q), 124.4 (t), 124.3 (t), 123.3 (t), 123.2 (t), 122.14 (t), 122.05 (t), 121.99 (t), 70.6 (p), 62.4 (p), 55.2 (t), 34.7 (q), 34.6 (q), 31.4 (p), 31.3 (p), 26.7 (q), 16.2 ppm (q); IR (ATR):

$\tilde{\nu} = 2959, 2862, 2833, 1481, 1363, 1306, 1263, 1149, 890, 871, 829, 797, 747, 605, 542, 489, 474\ cm^{-1}$; MS (MALDI, dithranol): m/z 1358.2 $[M^+]$, 1356.2, 1342.2, 1300.0; MS (ESI, 2-propanol): m/z 1358 $[M^+$ and $M_2^{2+}]$; elemental analysis: calcd (%) for $C_{98}H_{96}N_6$: C 86.68, H 7.13, N 6.19; found: C 86.59, H 7.18, N 6.09.

Single crystal X-ray diffraction

Single crystals suitable for X-ray diffraction were grown by slow diffusion of ethanol into a solution of receptor **7** in 1,2-dichlorobenzene. X-ray data for the single crystal structure determination of the chiral receptor were collected on a Bruker D8 Venture diffractometer. The frames were integrated with the Bruker SAINT software package using a narrow-frame algorithm. The integration of the data using an orthorhombic unit cell yielded a total of 61558 reflections to a maximum θ angle of $25.09°$ (0.84 Å resolution), of which 15453 were independent (average redundancy 3.993, completeness $= 99.8\%$, $R_{int} = 7.25\%$, $R_{sig} = 6.32\%$) and 11319 (73.86%) were greater than 2σ (F^2). The final cell constants of $a = 17.5092(15)$, $b = 21.167(2)$, $c = 23.599(2)$ Å, volume $= 8746.2(14)$ Å^3, are based upon the refinement of the XYZ-centroids of reflections above 20 $\sigma(I)$. The structure was solved and refined using SHELXS and SHELXL-97 programs,[33] using the space group $P2_12_12_1$ (no. 19), with $Z = 4$ for the formula unit, $C_{108}H_{105}Cl_2N_6O_2$. The final anisotropic full-matrix least-squares refinement on F^2 with 1041 variables converged at $R_1 = 8.22\%$, for the observed data and $wR_2 = 23.92\%$ for all data. The goodness-of-fit was 1.024. The largest peak in the final difference electron density synthesis was 0.637 e$^-$ Å^{-3} and the largest hole was -0.711 e$^-$ Å^{-3} with an RMS deviation of 0.069 e$^-$ Å^{-3}. On the basis of the final model, the calculated density was 1.187 g cm^{-3} and $F(000)$, 3408 e$^-$. Selected crystal data and details of structure refinement are provided in Table S3 in the Supporting Information. CCDC-1001598 contains the supplementary crystallographic data for this paper. These data can be obtained free of charge from The Cambridge Crystallographic Data Centre via www.ccdc.cam.ac.uk/data_request/cif.

VCD measurements of the chiral receptor

Compound **7** (3.2 mg) was dissolved in CDCl$_3$ (115 μL). The VCD spectra were recorded on a BioTools ChiralIR2X VCD spectrometer with the dual PEM setup optimized at 1400 cm^{-1}. The spectrum for solvent and sample were recorded separately in a detachable cell with BaF$_2$ windows and a 100 μm path. A resolution of 4 cm^{-1} was used throughout and 30000 scans were recorded. As only one absolute configuration of **7** was available, a solvent blank VCD spectrum was used for background corrections.

Electronic circular dichroism

ECD was also measured for receptor **7**. As solvent, 2,2,2-trifluoroethanol was used. Due to the low solubility and limited availability of **7**, no exact concentration could be established, but still a spectrum could be recorded between 200 and 400 nm. ECD spectra were measured on a Jasco J-710 spectrometer with a 1 mm optical path length cell.

Computational section

To compute the chiroptical spectra, the geometry of **7** was optimized at the B3LYP/6-31G*[34,35] level of theory using analytical gradients and an analytically computed initial Hessian. For the minimum found, VCD and ECD spectra were computed.[36] For VCD the B3LYP/6-31G* level of theory (1752 basis functions) was used, which corresponds to the highest level of theory affordable for the present size of compound on routinely available computers.[37,38] For the ECD spectrum, TDDFT B3LYP/6-31G* calculations include 150 excited states. To compare theoretical and experimental data, the theoretical spectra were broadened using a Lorentzian shape for VCD with a line width of 10 cm^{-1}. The scaling factor to align theoretical and experimental spectra was established by seeking the maximum similarity in the IR spectrum using the CompareVOA algorithm and program.[39] This resulted in a scale factor of 0.968. This scale factor compares fairly well with the B3LYP/6-31G* value in the NIST database (0.960).[40] For ECD, Gaussian broadening with a width of $\Delta = 6$ nm at 1/e of peak height was used.[41] All calculations were performed using the Gaussian 09 program.[42]

All molecular dynamics simulations were carried out using the pydlpoly package,[30] in the NVT ensemble with a fully atomistic first-principles parameterized force field. The force field in this work has been introduced in detail elsewhere.[30] For the extension of the force field used in ref. [14], reference calculations have been performed with the TURBOMOLE (V6.3) package[43] on the B3LYP/cc-pVDZ level, which is the standard procedure for MOF-FF. From these atomic charges were derived and the bonded parameters were fitted by a Genetic algorithm optimization method.[30]

To keep the dipolar group upright in the absence of a solvent, that is, perpendicular to the C_3 symmetry axis of the receptor, we added a soft harmonic angle restraint between the central sp^3 carbon of the receptor, the center of mass of the C$_{60}$ fragment and the top nitrogen atom of the rotor with an equilibrium angle of 180° and a small force constant of 0.1 kcal mol^{-1} rad^{-1}. The restraint energy at the 90° bent global minimum in the gas phase is about 14 kcal mol^{-1}, which roughly compensates the dispersive interaction energy between the dipolar group and the receptor and hence prevents the dipolar group to become entangled between the receptor arms. To enforce a stepwise rotation of the dipolar group around the C_3 symmetry axis we used a harmonic dihedral constrain between nitrogen atom of the NO$_2$ group, the top middle nitrogen atom of the dipolar group, the center of mass of the C$_{60}$ fragment and one of the neighboring carbon atoms of the receptor connected to the *tert*-butyl group. The force constant for the dihedral constrain was taken to be 10 kcal mol^{-1} rad^{-1}.

[1] a) V. Balzani, M. Gómez-López, J. F. Stoddart, *Acc. Chem. Res.* **1998**, *31*, 405–414; b) V. Balzani, A. Credi, F. M. Raymo, J. F. Stoddart, *Angew. Chem.* **2000**, *112*, 3484–3530; *Angew. Chem. Int. Ed.* **2000**, *39*, 3348–3391; c) *Top. Curr. Chem.* **2005**, *262*; special volume on *Molecular Machines* (Ed.: T. R. Kelly); d) W. R. Browne, B. L. Feringa, *Nat. Nanotechnol.* **2006**, *1*, 25–35; e) A. Mateo-Alonso, D. Guldi, F. Paolucci, M. Prato, *Angew. Chem.* **2007**, *119*, 8266–8272; *Angew. Chem. Int. Ed.* **2007**, *46*, 8120–8126.

[2] a) R. Feynman, R. B. Leighton, M. Sands, *The Feynman Lectures on Physics, Vol. 1* Addison–Wesley, Reading, MA, **1963**, chap. 46–1; b) R. D. Astumian, *Science* **1997**, *276*, 917–922; c) A. P. Davis, *Angew. Chem.* **1998**, *110*, 953–954; *Angew. Chem. Int. Ed.* **1998**, *37*, 909–910; d) *Stochastic Processes in Physics, Chemistry, and Biology: Lecture Notes in Physics* (Eds: J. A. Freund, T. Pöschel), Springer, Berlin, **2000**; e) R. D. Astumian, P. Hänggi, *Phys. Today* **2002**, *55*, 33–39; f) P. Hänggi, F. Marchesoni, F. Nori, *Ann. Phys.* **2005**, *14*, 51–70; g) A. P. Davis, *Nat. Nanotechnol.* **2007**, *2*, 135–136; h) P. Hänggi, F. Marchesoni, *Rev. Mod. Phys.* **2009**, *81*, 387–442.

[3] a) G. Vives, A. Carella, S. Sistach, J.-P. Launay, G. Rapenne, *New J. Chem.* **2006**, *30*, 1429–1438; b) G. Vives, A. Gonzalez, J. Jaud, J.-P. Launay, G. Rapenne, *Chem. Eur. J.* **2007**, *13*, 5622–5631; c) A. Carella, C. Coudret, G. Guirado, G. Rapenne, G. Vives, J.-P. Launay, *Dalton Trans.* **2007**, 177–186; d) H.-P. J. de Rouville, G. Vives, G. Rapenne, *Pure Appl. Chem.* **2008**, *80*, 659–667.

[4] a) T. R. Kelly, H. De Silva, R. A. Silva, *Nature* **1999**, *401*, 150–152; b) T. R. Kelly, R. A. Silva, H. De Silva, S. Jasmin, Y. Zhao, *J. Am. Chem. Soc.* **2000**, *122*, 6935–6949; c) S. P. Fletcher, F. Dumur, M. M. Pollard, B. L. Feringa, *Science* **2005**, *310*, 80–82.

[5] a) N. Koumura, R. W. J. Zijlstra, R. A. van Delden, N. Harada, B. L. Feringa, *Nature* **1999**, *401*, 152–155; b) R. A. van Delden, M. K. J. ter Weil, M. M. Pollard, J. Vicario, N. Koumura, B. L. Feringa, *Nature* **2005**, *437*, 1337–1340; c) M. M. Pollard, M. Lubomska, P. Rudolf, B. L. Feringa, *Angew. Chem.* **2007**, *119*, 1300–1302; *Angew. Chem. Int. Ed.* **2007**, *46*, 1278–1280; d) A. Cnossen, L. Hou, M. M. Pollard, P. V. Wesenhagen, W. R. Browne, B. L. Feringa, *J. Am. Chem. Soc.* **2012**, *134*, 17613–17619.

[6] N. Ruangsupapichat, M. M. Pollard, S. R. Harutyunyan, B. L. Feringa, *Nat. Chem.* **2011**, *3*, 53–60.

[7] T. Kudernac, N. Ruangsupapichat, M. Parschau, B. Macia, N. Katsonis, S. R. Harutyunyan, K.-H. Ernst, B. L. Feringa, *Nature* **2011**, *479*, 208–211.

[8] a) Y. Amatatsu, *J. Phys. Chem. A* **2011**, *115*, 13611–13618; b) Y. Amatatsu, *J. Phys. Chem. A* **2012**, *116*, 10182–10193.

[9] a) H. Tutu, S. Nagata, *Phys. Rev. E* **2013**, *87*, 022144; b) J. Lim, J. E. Sader, P. Mulvaney, *Phys. Rev. E* **2009**, *79*, 030105(R); c) F. Renzoni, *Adv. At. Mol. Opt. Phys.* **2009**, *57*, 1–32; d) E. R. Kay, D. A. Leigh, F. Zerbetto, *Angew. Chem.* **2007**, *119*, 72–196; *Angew. Chem. Int. Ed.* **2007**, *46*, 72–191; e) P. Reimann, *Phys. Rep.* **2002**, *361*, 57–265; f) K. Kinbara, T. Aida, *Chem. Rev.* **2005**, *105*, 1377–1400.

[10] E. Espildora, J. L. Delgado, P. de La Cruz, A. de La Hoz, V. Lopez-Arza, F. Langa, *Tetrahedron* **2002**, *58*, 5821–5826.

[11] a) F. Diederich, M. Gómez-López, *Chem. Soc. Rev.* **1999**, *28*, 263–277; b) T. Seidemann, *J. Phys. Condens. Matter* **2003**, *15*, R521–549; c) N. Martín, J.-F. Nierengarten, *Tetrahedron* **2006**, *62*, 1917.

[12] B. Bredenkötter, S. Henne, D. Volkmer, *Chem. Eur. J.* **2007**, *13*, 9931–9938.

[13] S. Henne, B. Bredenkötter, A. A. D. Baghi, R. Schmid, D. Volkmer, *Dalton Trans.* **2012**, *41*, 5995–6002.

[14] S. Henne, B. Bredenkötter, M. Alaghemandi, S. Bureekaew, R. Schmid, D. Volkmer, Almost Enclosed Buckyball Joints: Synthesis Complex Formation and Computational Simulations of a Pentypticene-Extended Tribenzotriquinacene, unpublished results.

[15] R. Schwenninger, Y. Ramondenc, K. Wurst, J. Schlögl, B. Kräutler, *Chem. Eur. J.* **2000**, *6*, 1214–1223.

[16] J. D. Bacha, J. K. Kochi, *Tetrahedron* **1968**, *24*, 2215–2226.

[17] J. Tellenbröker, D. Kuck, *Angew. Chem.* **1999**, *111*, 1000–1004; *Angew. Chem. Int. Ed.* **1999**, *38*, 919–922.

[18] J. Tellenbröker, D. Kuck, *Beilstein J. Org. Chem.* **2011**, *7*, 329–337.

[19] J. Strübe, B. Neumann, H.-G. Stammler, D. Kuck, *Chem. Eur. J.* **2009**, *15*, 2256–2260.

[20] T. Wang, Y.-F. Zhang, Q.-Q. Hou, W.-R. Xu, X.-P. Cao, H.-F. Chow, D. Kuck, *J. Org. Chem.* **2013**, *78*, 1062–1069.

[21] a) H. D. Flack, G. Bernardinelli, *Chirality* **2008**, *20*, 681–690; b) H. D. Flack, *Acta Chim. Slov.* **2008**, *55*, 689–691; c) H. D. Flack, G. Bernardinelli, *J. Appl. Cryst.* **2000**, *33*, 1143–1148; d) H. D. Flack, G. Bernardinelli, *Acta Crystallogr. A* **1999**, *55*, 908–915.

[22] P. Polavarapu, N. Jeirath, T. Kurtan, G. Pescitelli, K. Krohn, *Chirality* **2009**, *21*, E202–E207.

[23] Molecular Weight Calculator, Version 6.48.

[24] W. G. Barb, *Trans. Faraday Soc.* **1953**, *49*, 143–148.

[25] C. W. Davis, *Ion Association*, Butterworth, Washington D.C., **1962**, p.41.

[26] B. Dodson, R. Foster, A. A. S. Bright, M. I. Foreman, J. Gorton, *J. Chem. Soc. B* **1971**, 1283–1293.

[27] A. Job, *Ann. Chim.* **1929**, *9*, 113.

[28] K. A. Connors, *Binding Constants*, Wiley, New York, **1987**.

[29] T. Wang, Z.-Y. Li, A.-L. Xie, X.-J. Yao, X.-P. Cao, D. Kuck, *J. Org. Chem.* **2011**, *76*, 3231–3238.

[30] S. Bureekaew, S. Amirjalayer, M. Tafipolsky, C. Spickermann, T. K. Roy, R. Schmid, *Phys. Status Solidi B* **2013**, *250*, 1128–1141.

[31] S. Doherty, J. G. Knight, A. L. Bell, R. W. Harrington, W. Clegg, *Organometallics* **2007**, *26*, 2465–2468.

[32] D. Maag, T. Kottke, M. Schulte, A. Godt, *J. Org. Chem.* **2009**, *74*, 7733–7742.

[33] G. M. Sheldrick, SHELXL-97, Program for Refinement of Crystal Structures, University of Göttingen, Germany, **1997**.

[34] a) A. D. Becke, *J. Chem. Phys.* **1993**, *98*, 5648–52; b) C. Lee, W. Yang, R. G. Parr, *Phys. Rev. B* **1988**, *37*, 785–789; c) P. J. Stephens, F. J. Devlin, C. F. Chabalowski, M. J. Frisch, *J. Phys. Chem.* **1994**, *98*, 11623–11627.

[35] R. Ditchfield, W. J. Hehre, J. A. Pople, *J. Chem. Phys.* **1971**, *54*, 724–728.

[36] a) P. J. Stephens, *J. Phys. Chem.* **1985**, *89*, 748–752; b) J. R. Cheeseman, M. J. Frisch, F. J. Devlin, P. J. Stephens, *Chem. Phys. Lett.* **1996**, *252*, 211–220.

[37] T. Kuppens, W. Langenaeker, J. P. Tollenaere, P. Bultinck, *J. Phys. Chem. A* **2003**, *107*, 542–553.

[38] L. A. Nafie, *Vibrational Optical Activity: Principles and Applications 1st ed.*, Wiley, New York, **2011**.

[39] a) E. Debie, E. De Gussem, R. K. Dukor, W. Herrebout, L. A. Nafie, P. Bultinck, *ChemPhysChem* **2011**, *12*, 1542–1549; b) T. Kuppens, K. Vandyck, J. Van der Eycken, W. Herrebout, B. J. van der Veken, P. Bultinck, *J. Org. Chem.* **2005**, *70*, 9103–9114.

[40] National Institute of Standards and Technology Computational Chemistry Comparison and Benchmark DataBase Release 15b, August **2011**, NIST Standard Reference Database 101.

[41] P. J. Stephens, N. Harada, *Chirality* **2010**, *22*, 229–233.

[42] Gaussian 09 (Revision B.01), M. J. T. Frisch, G. W. Schlegel, H. B. Scuseria, G. E. Robb, M. A. Cheeseman, J. R. Scalmani, G. Barone, V. Mennucci, B. Petersson, G. A. Nakatsuji, H. Caricato, M. Li, X. Hratchian, H. P. Izmaylov, A. F. Bloino, J. Zheng, G. Sonnenberg, J. L. Hada, M. Ehara, M. Toyota, K. Fukuda, R. Hasegawa, J. Ishida, M. Nakajima, T. Honda, Y. Kitao, O. Nakai, H. Vreven, T. Montgomery, Jr., J. A. Peralta, J. E. Ogliaro, F. Bearpark, M. Heyd, J. J. Brothers, E. Kudin, K. N. Staroverov, V. N. Kobayashi, R. Normand, J. Raghavachari, K. Rendell, A. Burant, J. C. Iyengar, S. S. Tomasi, J. Cossi, M. Rega, N. Millam, N. J. Klene, M. Knox, J. E. Cross, J. B. Bakken, V. Adamo, C. Jaramillo, J. Gomperts, R. Stratmann, R. E. Yazyev, O. Austin, A. J. Cammi, R. Pomelli, C. Ochterski, J. W. Martin, R. L. Morokuma, K. Zakrzewski, V. G. Voth, G. A. Salvador, P. Dannenberg, J. J. Dapprich, S. Daniels, A. D. Farkas, Ö. Foresman, J. B. Ortiz, J. V. Cioslowski, J. Fox, D. J. Gaussian, Inc., Wallingford CT, **2009**.

[43] TURBOMOLE V6.3 2011, a development of University of Karlsruhe and Forschungszentrum Karlsruhe GmbH, **1989–2007**, TURBOMOLE GmbH, since 2007 available from http://www.turbomole.com.